Degree Project in Technology

First Cycle, 15 credits

Insights into 2D Navier-Stokes Numerical Simulations

Energy-Conserving Solver Approaches

ANGELICA SAVVIDIS, MIRANDA KOLOUH WESTIN

Abstract

Understanding the behavior of viscous incompressible fluids is essential for scientific applications, yet when modeling them presents significant theoretical and practical challenges. This study aimed to develop a numerical solver especially for the two-dimensional Navier-Stokes equation, tailored for modeling the dynamics of a viscous incompressible fluid, to conserve the enstrophy. The goal was to accurately simulate a physical system, and apply numerical methods such as Runge-Kutta 4, Forward Euler's method, and pseudo-spectral methods to construct and solve the governing Partial Differential Equations (PDEs).

These methods were evaluated for their ability to conserve the enstrophy. Not only enhancing our understanding of the application of the equation in real physical systems, this research also contributes to expanding the understanding of numerical methodologies for complicated PDEs in physical simulations.

Using the aforementioned methods, together with strategically specific initial conditions, it is observable that the methods are sufficient for conserving the enstrophy when dealing with only the linear part of Navier-Stokes. To improve the numerical methods concerning the non-linear part of the Navier-Stokes, a perturbation method was implemented. Outcomes from this method appear promising however, implementation and more detailed analysis are not included in this report due to time constraints. This recovery strategy represents a foundation for further exploration in further research.

Keywords: Navier-Stokes 2D equation · Enstrophy conservation · Implicit- and Explicit methods

Contents

1 Introduction

Fluid dynamics plays an important role in both natural environments and engineered systems, governed by the Navier-Stokes equations. These equations support many natural and industrial processes, yet accurately simulating these phenomena remains one of the grand challenges in computational physics. It is a foundation for understanding turbulent flows, and pattern formations and causes unique challenges due to the necessity of conserving quantities like enstrophy — an essential feature for maintaining physical credibility in simulations.

The conservation of physical quantities such as kinetic energy and enstrophy is necessary to capture underlying dynamics. Ensuring numerical stability and achieving accurate results implies that vital properties are preserved in the computational models.

Discretization methods are used for approximating continuous functions, differential equations, or integrals in a discrete form. Even though these numerical methods are designed to preserve some quantities there exists limitations and truncation in these processes that can lead to unintended errors, such as artificial energy loss [1]. This phenomenon refers to where the numerical scheme shows a loss (or a gain) of energy that is not present in a real modeled system. This deviation appears from numerical errors, approximations made in the discretization process, or the inability of the numerical method to capture the complicated dynamics of the system.

The goal of this study is to enhance the numerical time-stepping solvers; Forward Euler and Runge-Kutta 4, for the two-dimensional (2D) Navier-Stokes equation, and to evaluate these solvers based on their conservation of enstrophy. These methods are not as renowned for preserving such quantities as for methods like staggering and skew-symmetrization of the convective terms [1]. However, the question of interest is whether it is possible to implement a complementary strategy to the numerical methods so they conserve energy quantities.

The partial differential equation being analyzed is the vorticity-streamfunction formulation of the Navier-Stokes equation, which includes both a linear and nonlinear term. The linear term is studied using the Taylor-Green initial condition and the non-linear term is investigated using a random vorticity field as an initial condition. The vorticity in the Navier-Stokes equation is numerically solved with a spatial discretization in Fourier space and time stepping with Forward Euler and Runge-Kutta 4. The enstrophy is then calculated and compared to a manifold.

Due to larger relative errors in the non-linear solution, a strategy for enhancing the numerical methods ability to conserve the enstrophy is tested. The strategy is to use an asymptotic expansion with a perturbed function that is orthogonal to the manifold. This strategy aims to find an orthogonal function to project the numerical approximation onto and then use retraction mapping to get a more accurate solution. The result of the perturbation method shows that it is a good method that can be used to improve the numerical solvers when dealing with non-linear PDEs.

The 2D Navier-Stokes equation and the selected initial condition are introduced in Section 2. The spatial and time discretization is implemented in Section 3. The asymptotic expansion with the aforementioned perturbation method which is implemented to conserve the enstrophy in the numerical methods is explored in Section 4. Computational results are presented in Section 5.1, whereas discussion and conclusions are deferred to Section 6.

2 The Navier-Stokes System

2.1 The Navier-Stokes 2D equation

The Navier-Stokes equations are a set of partial differential equations (PDEs), cf eq. (1), which can be applied to solve fluid flow problems [2]. The equations are useful in developing numerical models for fluid dynamics. Depending on which flow characteristics are being analyzed, the Navier-Stokes equations can be evaluated in various dimensions. In this study, the focus is on the incompressible two-dimensional (2D) Navier-Stokes equation. The velocity-pressure formulation is represented below by 1a. The incompressible condition is ensured by 1b which is a result of a vector field with the divergence zero at all points - solenoidal velocity field [3]. For simplicity the spatial domain Ω, is being considered as a periodic box, $\Omega \in [0, 2\pi] \times [0, 2\pi]$, and can be written as

$$\mathbf{u}_t + \mathbf{u} \cdot \boldsymbol{\nabla}\mathbf{u} + \frac{1}{\rho}\boldsymbol{\nabla}p - \nu\ \boldsymbol{\Delta}\mathbf{u} = \mathbf{f} \qquad \text{in } (0,T] \times \Omega, \tag{1a}$$

$$\boldsymbol{\nabla} \cdot \mathbf{u} = 0 \qquad \text{in } (0,T] \times \Omega, \tag{1b}$$

$$\mathbf{u}(t=0) = \mathbf{u}_0 \qquad \text{in } \Omega, \tag{1c}$$

where, $\mathbf{u} = [u_x, u_y, 0]^T$ is the velocity of the fluid, p is the pressure and ν is the kinematic viscosity.

Furthermore, there are no external forcing considered in this study, therefore, $f = 0$. The kinematic viscosity, ν is a constant and the density ρ is assumed to be of a constant value $\rho = 1$, without loss of generality. With these assumptions, 1 can be expressed in a simpler form

$$\mathbf{u}_t + \mathbf{u} \cdot \boldsymbol{\nabla}\mathbf{u} + \boldsymbol{\nabla}p - \nu\boldsymbol{\Delta}\mathbf{u} = 0 \qquad \text{in } (0,T] \times \Omega, \tag{2a}$$

$$\boldsymbol{\nabla} \cdot \mathbf{u} = 0 \qquad \text{in } (0,T] \times \Omega, \tag{2b}$$

$$\mathbf{u}(t=0) = \mathbf{u}_0 \qquad \text{in } \Omega. \tag{2c}$$

The vorticity $\boldsymbol{\omega}$ of a fluid describes how much a fluid swirls and is defined by taking the curl of the velocity [4]. The vorticity-velocity formulation of the Navier-Stokes equation arises by taking the curl of eq. (2)

$$\boldsymbol{\omega}_t + \mathbf{u} \cdot \boldsymbol{\nabla}\boldsymbol{\omega} + \boldsymbol{\omega} \cdot \boldsymbol{\nabla}\mathbf{u} - \nu\boldsymbol{\Delta}\boldsymbol{\omega} = 0 \qquad \text{in } (0,T] \times \Omega, \tag{3a}$$

$$\boldsymbol{\Delta} \cdot \mathbf{u} = -\boldsymbol{\nabla} \times \boldsymbol{\omega} \qquad \text{in } (0,T] \times \Omega, \tag{3b}$$

$$\boldsymbol{\omega}(t=0) = \boldsymbol{\omega}_0 \qquad \text{in } \Omega. \tag{3c}$$

It can be noted that when the curl operator is applied to the pressure component it is eliminated, eq. (5a). Furthermore, since we are considering this as a 2D flow, the vorticity vector only has one nonzero component, as

$$\begin{aligned} \boldsymbol{\omega} = \boldsymbol{\nabla} \times \mathbf{u} &= \begin{vmatrix} \hat{\mathbf{i}} & \hat{\mathbf{j}} & \hat{\mathbf{k}} \\ \frac{\partial}{\partial x} & \frac{\partial}{\partial y} & 0 \\ u_x & u_y & 0 \end{vmatrix}, \\ &= (0-0)\,\hat{\mathbf{i}} - (0-0)\,\hat{\mathbf{j}} + \left(\frac{\partial u_y}{\partial x} - \frac{\partial u_x}{\partial y}\right)\hat{\mathbf{k}}, \\ &= \omega_z \mathbf{k} = \omega. \end{aligned} \tag{4}$$

Because of this the term $(\omega \cdot \nabla\mathbf{u})$, known as the vortex stretching, from eq. (3) is zero

$$\boldsymbol{\nabla} \times \boldsymbol{\nabla} p = \begin{bmatrix} \frac{\partial}{\partial x_1} \\ \frac{\partial}{\partial x_2} \\ 0 \end{bmatrix} \times \begin{bmatrix} \frac{\partial p}{\partial x_1} \\ \frac{\partial p}{\partial x_2} \\ 0 \end{bmatrix} = 0, \tag{5a}$$

$$\boldsymbol{\omega} \cdot \boldsymbol{\nabla}\mathbf{u} = \begin{bmatrix} 0 \\ 0 \\ \omega \end{bmatrix} \cdot \begin{bmatrix} \frac{\partial u_{x_1}}{\partial x_1} & \frac{\partial u_{x_1}}{\partial x_2} & 0 \\ \frac{\partial u_{x_2}}{\partial x_1} & \frac{\partial u_{x_2}}{\partial x_2} & 0 \\ 0 & 0 & 0 \end{bmatrix} = 0. \tag{5b}$$

By removing the zero term from 3a, it allows a simpler formulation of the Navier-Stokes vorticity-velocity PDE in 2D

$$\omega_t + \mathbf{u} \cdot \nabla\omega - \nu\,\Delta\omega = 0. \tag{6}$$

Since the density is a constant and the fluid is incompressible, a way to further simplify 6 is to introduce the stream function ψ. The stream function is a scalar function that can be used to describe the velocity. Instead of having two unknown components (u_{x_1}, u_{x_2}) the stream function reduces the problem to one unknown scalar component [5].

The relation between the stream function, velocity, and vorticity can be described with

the Biot-Savart Law. This law was originally formulated to describe the magnetic field generated by a steady electric current, but the mathematical similarity between the description of velocity fields around vortex lines makes this law very usable in fluid dynamics [6]. The definition of this law is introduced below.

$$\begin{cases} -\omega = \boldsymbol{\Delta}\psi, \\ \mathbf{u} = \boldsymbol{\nabla}^{\perp}\psi, \\ \boldsymbol{\nabla}^{\perp} = \left(-\dfrac{\partial}{\partial y}, \dfrac{\partial}{\partial x}\right). \end{cases} \tag{7}$$

Implementing 7 in 6 introduces a new description of the Navier-Stokes equation in 2D. This formulation is called vorticity-streamfunction form, as mentioned in the thesis by Matharu [7],

$$\omega_t + \boldsymbol{\nabla}^{\perp}\psi \cdot \boldsymbol{\nabla}\omega - \nu\boldsymbol{\Delta}\omega = 0 \qquad \text{in } (0,T]\times\Omega, \tag{8a}$$

$$\boldsymbol{\Delta}\psi = -\omega \qquad \text{in } (0,T]\times\Omega, \tag{8b}$$

$$\omega(t=0) = \omega_0 \qquad \text{in } \Omega, \tag{8c}$$

and it is the equation which will be of main focus throughout this thesis. We note that in this study, the mean of the initial condition $\int_\Omega \omega_0(\mathbf{x})\, d\mathbf{x}$ is set to zero to guarantee that the Laplacian in 8b can be inverted within the periodic domain Ω when implementing the numerical methods [7].

This analysis examines both the linear- $(-\nu\Delta\omega)$ and non-linear term $(\nabla^{\perp}\psi \cdot \nabla\omega)$ from 8. To accurately identify these terms, it is essential to assume two scenarios: One where the fluid is viscous $(\nu > 0)$, and another where the fluid is inviscid $(\nu = 0)$ which corresponds to Euler's equation [7].

With the Navier-Stokes equation, we are focused on studying the energy quantities, more specifically the enstrophy of the system. The kinetic energy $\mathcal{K}$, enstrophy $\mathcal{E}$ and palinstrophy $\mathcal{P}$ is defined as

$$\mathcal{K}(\mathbf{u}) = \frac{1}{2}\int_\Omega \mathbf{u}(t,\mathbf{x})^2\, d\mathbf{x}, \tag{9}$$

$$\mathcal{E}(\omega) = \frac{1}{2}\int_{\Omega} \omega(t,\mathbf{x})^2 \, d\mathbf{x}, \tag{10}$$

$$\mathcal{P}(\omega) = \frac{1}{2}\int_{\Omega} (\nabla\omega(t,\mathbf{x}))^2 \, d\mathbf{x}, \tag{11}$$

where the enstrophy is proportional to the $L^2(\Omega)$ norm of vorticity,

$$\mathcal{E}(\omega) = \frac{1}{2}\int_{\Omega} \omega(t,\mathbf{x})^2 \, d\mathbf{x} = \frac{1}{2}\|\omega\|_{L^2(\Omega)} := \langle \omega, \omega \rangle_{L^2(\Omega)}. \tag{12}$$

A way to further analyze the enstrophy's behavior is to take the time derivative of 10. The expression is derived with integration by parts together with implementing 6. Deriving an expression can provide a clear understanding of the underlying principles and relationships within a system, enabling prediction and control of its behavior.

$$\begin{aligned} \frac{\partial \mathcal{E}}{\partial t} &= -\nu \int_{\Omega} (\nabla\omega(t,\mathbf{x}))^2 \, d\mathbf{x} \\ &= -2\nu\mathcal{P}(\omega). \end{aligned} \tag{13}$$

Equation (13) informs that the enstrophy is strictly dissipative over time when the kinetic viscosity, ν, is greater than zero. In the inviscid case ($\nu = 0$), the enstrophy remains constant. When we numerically approximate the vorticity based on 8, we check the performance of the numerical methods based on this behavior of the enstrophy.

2.2 Initial conditions

The performance of the numerical models was tested by testing a set of different initial conditions (IC). A way to tackle the terms from 8 could be done by using the well-known splitting method, which is a method that divides complicated equations into simpler, manageable sub-equations. This technique is proven effective for PDEs containing both linear and nonlinear terms [8]. Consequently, this method was selected for this study.

This method is applied in this study by studying the linear term $\mathcal{L}$

$$\omega_t^L = \nu\Delta\omega = \mathcal{L}(t,\mathbf{x}), \tag{14}$$

and the non-linear term $\mathcal{N}$

$$\omega_t^N = -\nabla^{\perp}\psi \cdot \nabla\omega = \mathcal{N}(t,\mathbf{x}), \tag{15}$$

separately. By using a smart choice of initial conditions and viscosities this is feasible. The choices of initial conditions for each term are introduced in the subsections to follow.

2.2.1 Linear term - Taylor-Green Vortex

A good choice of an IC for the evaluation of the linear term is the 2D Taylor-Green Vortex, which results in the non-linear term vanishing, thereby isolating the linear terms for study.
The initial condition and the analytical solution are given by

$$\omega(t=0,\mathbf{x}) = \omega_0 = A\,sin(a\,x_1)sin(b\,x_2), \tag{16a}$$

$$\omega(t,\mathbf{x}) = \omega_0\,e^{-2\nu t}, \tag{16b}$$

where A, a, b are constants that can be chosen freely. In this study, the standard constants were chosen as $A = 10, a = b = 2$. But when variations of other parameters were studied the constants were sometimes reformed if necessary. Equation (16b) allows a clear understanding of the effects of viscosity and time on the evolution of vorticity in the fluid.

Despite the simplicity of the Taylor-Green vortex, it summarizes the essential dynamics of fluid flow in a form that is both solvable and physically interesting. It demonstrates how the vorticity of a fluid evolves and interacts under the influence of its velocity field and viscosity, by simple dynamics of the heat equation.

In summary, the Taylor Green vortex provides a clear analytical model that captures the key dynamics of fluid flow. Because of this, it is a good model for comparison between the analytic solution and the numerical approximations, which will be introduced later in Section 3.

2.2.2 Non-Linear term - Random Vorticity Field

To analyze the behavior of the non-linear term the kinetic viscosity ν was set to zero to ensure the elimination of the linear term.
Various ICs were explored such as Jeong-Yenoda IC, a three-vortex setup, and a randomly generated initial condition, all designed by Matharu [7]. However, the initial condition of focus in this thesis is the randomly generated vorticity field.

The random vorticity field was constructed by creating a discretized grid which numerically represents a continuous field. The vorticity is divided into a grid of discrete points at which the equations are solved. This is crucial because it enables the transformation of continuous PDEs into solvable algebraic forms. This field was then generated in the Fourier space using random phases and controlled spectral decay, to help manage the numerical stability and accuracy of the simulations when it is afterward transformed

back to physical space. The resulting field is then normalized to have a L^2 norm so it is easier for comparison later. This normalization involves adjusting the amplitude of the field. This is also constructed to have a mean zero so the Laplacian can be inverted in eq. (8), so the sum of the squares of all values over the grid equals one.

The random initial condition was constructed in Fourier space as

$$\hat{\omega}(\boldsymbol{k}) = e^{i\xi} e^{-r\boldsymbol{k}}, \tag{17}$$

where i is the imaginary number, $\mathbf{k}$ is the wave vector and ξ are randomly distributed numbers from the interval $[-\pi, \pi]$.

3 Numerical Methods and Algorithms

To numerically solve eq. (8), the PDE must be discretized in both spatial and temporal dimensions. A Fourier-based method, more specifically a pseudo-spectral method is chosen for spatial discretization due to its efficiency in handling problems defined over periodic domains. For temporal discretization, the first-order Forward Euler's method and the fourth-order Runge-Kutta 4 method is used. The time discretization methods are chosen because of their simplicity. It is known that they are a sub-optimal choice for conserving certain quantities of energy, but the main goal in this study, as mentioned in Section 1 is to investigate how they eventually could conserve the quantities of interest through simple modifications.

3.1 Spatial Discretization

The solution $\omega(\mathbf{x}, t)$ is expressed as a sum of basis functions using Fourier with the 2D wave vectors $\mathscr{K} = \{\mathbf{k} \in \mathbb{Z}^2 : |\mathbf{k}| \leq K\}$, where K is the maximum wavenumber [7]. The vorticity can then be expressed as

$$\omega(t, \mathbf{x}) = \sum_{k \in \mathscr{K}} \hat{\omega}(t, \mathbf{k})\, e^{i\mathbf{k}\mathbf{x}} = \sum_{k \in \mathscr{K}} \hat{\omega}_{k_1 k_2}(t)\, e^{i(k_1 x_1 + k_2 x_2)}, \tag{18}$$

where $\hat{\cdot}$ is used to denote Fourier space and $\hat{\omega}_k(t)$ are the Fourier coefficients.

To express eq. (8) in Fourier space we describe the PDE as

$$\frac{\partial \hat{\omega}(t, \mathbf{k})}{\partial t} = \hat{\mathcal{N}}(t, \hat{\omega}) + \hat{\mathcal{L}}(t, \hat{\omega}), \tag{19}$$

where the linear term in Fourier space is represented as $\hat{\mathcal{L}}$ and the non-linear term in Fourier space as $\hat{\mathcal{N}}$. From now on the right-hand side of eq. (19) will be denoted as $g(t, \hat{\omega_k})$. This is used in the time-stepping with the numerical methods.
The linear term in eq. (19) is computed in Fourier space and can be written as

$$\mathcal{L}(t, \hat{\omega}) = -\nu \left(\sum_{k \in \mathscr{K}} |\mathbf{k}|^2\, \hat{\omega}(t, \mathbf{k}) \right), \tag{20}$$

and $\mathcal{N}$ in eq. (19), is implemented using a pseudo-spectral method with dealiasing,

$$\mathcal{N}(t, \omega(\mathbf{x})) = \frac{\partial \psi(t, \mathbf{x})}{\partial x_2} \frac{\partial \omega(t, \mathbf{x})}{\partial x_1} - \frac{\partial \psi(t, \mathbf{x})}{\partial x_1} \frac{\partial \omega(t, \mathbf{x})}{\partial x_2}, \tag{21}$$

where the definition of the terms in eq. (21) is defined in Fourier space as [7]

$$\frac{\partial \psi(t,\mathbf{x})}{\partial x_1} = \sum_{k\in\mathscr{K}} (ik_1)\hat{\psi}(t,\mathbf{k})e^{i\mathbf{k}x}, \tag{22a}$$

$$\frac{\partial \psi(t,\mathbf{x})}{\partial x_2} = \sum_{k\in\mathscr{K}} (ik_2)\hat{\psi}(t,\mathbf{k})e^{i\mathbf{k}x}, \tag{22b}$$

$$\frac{\partial \omega(t,\mathbf{x})}{\partial x_1} = \sum_{k\in\mathscr{K}} (ik_1)\hat{\omega}(t,\mathbf{k})e^{i\mathbf{k}x}, \tag{22c}$$

$$\frac{\partial \omega(t,\mathbf{x})}{\partial x_2} = \sum_{k\in\mathscr{K}} (ik_2)\hat{\omega}(t,\mathbf{k})e^{i\mathbf{k}x}. \tag{22d}$$

As highlighted in the study by Matharu [7], the transformation of the non-linear term eq. (21), needs to be dealiased to maintain numerical accuracy. This is usually achieved through the application of a Gaussian filter [9]. In this study, we adopt a similar approach to reduce potential numerical instabilities that can occur with the pseudo-spectral method. Implementing the Gaussian filter, ensures that the spectrum of the model is preserved, preventing the instabilities of the numerical methods that can occur.

The non-linear term is initially computed in the physical space, by calculation of the derivatives of the vorticity and the stream function. The non-linear term is then transformed back to Fourier space, where it is used in the time discretization methods. This approach, as documented in the study by Matharu [7], ensures that the transformations between physical and Fourier spaces are accurately handled, thereby maintaining the consistency and stability of the numerical methods implemented.

3.2 Time Discretization

For the discretization in time we try different numerical approximation methods to determine how well a simpler method preserves the enstrophy in comparison to a more complex one. We try both methods using different initial conditions from Section 2.2 to see exactly how the linear and non-linear terms behave and if the numerical solution satisfies eq. (10).

3.2.1 Forward Euler

From eq. (19) when discretization is performed in time and the Fourier coefficient updates at $t + \Delta t$ the Forward Euler equation is represented as

$$\hat{\omega}^{n+1} = \hat{\omega}^n + \Delta t \cdot g(t^n, \hat{\omega}^n), \tag{23}$$

where $g(t^n, \hat{\omega}^n)$ is the right hand side of eq. (19).

Euler's method is one of the oldest and is characterized by its simplicity and computational efficiency. However, there is a trade-off between simplicity and accuracy. The method only uses a single tangent line at the beginning of each time step, without taking the changes in the function's slope within itself into consideration. This can result in less accurate approximations [10].

3.2.2 Runge-Kutta 4

The Runge-Kutta method was formulated by Runge in 1894 and some years later it was extended by Kutta and is a more refined approach than Forward Euler [10].

The intermediate steps are calculated once for each increment of the function. The Runge-Kutta method of the fourth order updates the solution using four intermediate steps c_1, c_2, c_3, c_4, that are presented as

$$\begin{aligned} c_1 &= g(t^n, \hat{\omega}^n), \\ c_2 &= g(t^n, \hat{\omega}^n + \frac{c_1}{2}), \\ c_3 &= g(t^n, \hat{\omega}^n + \frac{c_2}{2}), \\ c_4 &= g(t^n, \hat{\omega}^n + c_3,). \end{aligned}$$

The Fourier coefficient at $t + \Delta t$ are then updated as

$$\hat{\omega}^{n+1} = \hat{\omega}^n + \frac{\Delta t}{6}(c_1 + 2c_2 + 2c_3 + c_4).$$

4 Strategy for conserving enstrophy

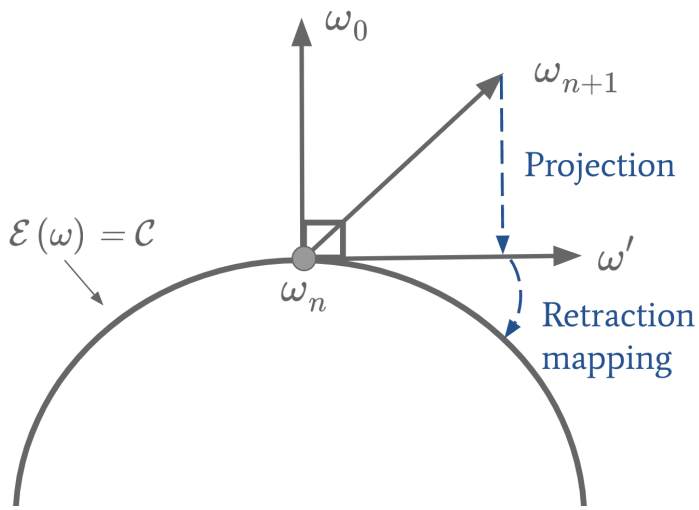

Figure 1: Illustrative figure of recovering strategy

Since the numerical methods are approximations it is interesting to explore ways to make the methods more accurate. We focus on an asymptotic expansion on the IC when $\nu = 0$. The objective is to numerically solve a perturbation that is orthogonal to the initial condition ω_0. If it is orthogonal, one can continue this study by projecting the numerical iteration ω^{n+1} onto the tangent space and then use retraction mapping to adjust the numerical approximation. This method is illustrated through Figure 1.

4.1 Asymptotic Expansion using Perturbations

In numerical problem solving, when a small perturbation is introduced to the initial condition, the technique is referred to as an asymptotic expansion. Following this approach, the modified IC can be expressed as

$$\omega_0 \leftarrow \omega_0 + h\,\omega_0', \tag{24}$$

where $0 < h \ll 1$ and ω_0' is a perturbed initial vorticity. The perturbation is a function within the Lebesgue space, L^2, and has a mean of zero. Based on this, the vorticity and the stream function can be expanded similarly, hence

$$\omega \leftarrow \omega + h\,\omega', \tag{25a}$$
$$\psi \leftarrow \psi + h\,\psi'. \tag{25b}$$

To simplify, the perturbation function was selected as

$$\omega'(\mathbf{x}) = e^{-x_1^2 - x_2^2}. \tag{26}$$

The new perturbed eq. (25) is inserted in eq. (8) and after collecting the h-terms the updated version of the differential equation is

$$\omega_t' + \nabla^\perp \psi \, \nabla \, \omega' + \nabla^\perp \psi' \nabla \, \omega = 0, \tag{27a}$$

$$\Delta \, \psi' = -\omega', \tag{27b}$$

$$\omega'(t=0) = \omega_0'. \tag{27c}$$

This equation can be solved with Forward Euler and Runge-Kutta 4 to get the approximated solution ω'.

The next part is to check that the Gâteaux derivative, expressed as a finite difference approximation of a derivative, goes to zero for some small h [11]

$$\mathcal{E}'(\omega_0, \omega') = \lim_{h \to 0} \frac{\mathcal{E}(\omega_0 + h\omega') - \mathcal{E}(\omega_0)}{h} = 0. \tag{28}$$

For the non-linear case it is known that analytically $\mathcal{E}(\omega) = \mathcal{E}(\omega_0)$. This implies

$$\frac{1}{2} \int \omega_0^2 \, d\vec{x} = \frac{1}{2} \int \omega^2 \, d\vec{x}, \tag{29}$$

therefore the relation $\mathcal{E}'(\omega_0; \omega') = \mathcal{E}'(\omega; \omega')$ is a confirmed expression.

Continuing with this strategy h needs to go to zero. This was accomplished by breaking down the integral

$$\begin{aligned} &\lim_{h \to 0} \frac{\mathcal{E}(\omega_0 + h\omega') - \mathcal{E}(\omega_0)}{h} \\ &= \lim_{h \to 0} \frac{1}{2h} \int_\Omega ((\omega_0 + h\omega')^2 - \omega_0^2) \, d\mathbf{x} \\ &= \lim_{h \to 0} \frac{1}{2} \int_\Omega (2\omega'\omega_0 + h\omega'^2) \, d\mathbf{x} \\ &= \int_\Omega \omega_0 \, \omega' \, d\mathbf{x}. \end{aligned} \tag{30}$$

The outcome of eq. (30) is that the inner product $\langle \omega, \omega' \rangle_{L^2(\Omega)}$ is equal to zero.

$$\langle \omega, \omega' \rangle_{L^2(\Omega)} = \lim_{h \to 0} \frac{\mathcal{E}(\omega_0 + h\omega') - \mathcal{E}(\omega_0)}{h}. \tag{31}$$

If eq. (31) is true for some h, it is proven that one can numerically solve a perturbation by using this approach to enhance the accuracy of numerical methods.

To compare the left- and right-hand side of eq. (31) the introduction of a new variable κ becomes essential. This variable should be equal to 1 for some h to see if the method works.

$$\kappa(h) = \frac{\lim_{h \to 0} \frac{\mathcal{E}(\omega_0 + h\omega') - \mathcal{E}(\omega_0)}{h}}{\langle \omega, \omega' \rangle_{L^2(\Omega)}} \approx 1, \tag{32a}$$

$$|\kappa(h) - 1| \approx 0. \tag{32b}$$

Lastly, eq. (32b) is evaluated for different h's to validate that intermediate values of h satisfy eq. (31).

5 Numerical Results

5.1 Enstrophy conservation with numerical methods

5.1.1 Enstrophy for the Linear Term

Initially, the enstrophy for the linear term from eq. (14) was derived from the Taylor-Green initial condition, as per eq. (16a), was compared with the enstrophy of the analytical solution detailed in eq. (16b). Consistent numerical parameters were set, the kinematic viscosity ($\nu = 10^{-4}$), the time domain ($T = 1$), and the spatial resolution in each direction ($N = 32$). Doing so isolates the impact of the time step variations on the accuracy and stability of the solution.

The results of the enstrophy for Forward Euler and Runge-Kutta 4 are presented in Figure 2.

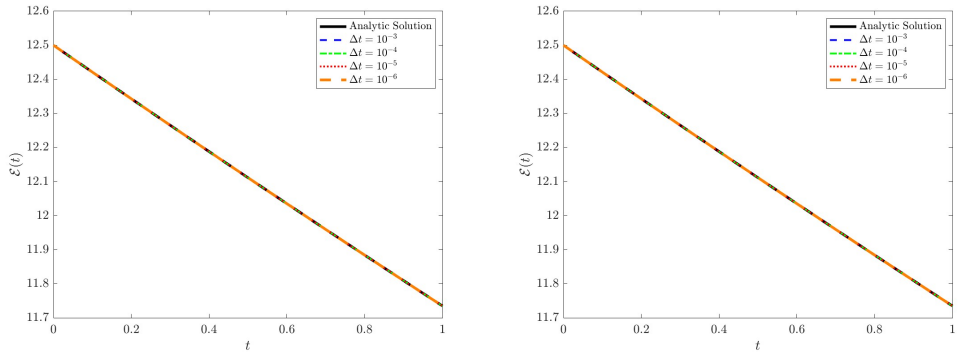

(a) Forward Euler **(b)** Runge-Kutta 4

Figure 2: Numerical result of Enstrophy for the linear term with different time steps

What is observed is that they appear to be accurate for all time steps when comparing them to the Taylor-Green "curve" which indicates that these methods are sufficient.

Since both Euler Forward and Runge-Kutta 4 show very similar behavior to each other and the analytic solution it is interesting to confirm this by checking the relative error, $\eta_{\mathcal{E}}$, between these methods separately and the analytic solution. Let $\tilde{\mathcal{E}} \approx \mathcal{E}$ be an approximation of $\mathcal{E}$. $\eta_{\mathcal{E}}$ is defined as

$$\eta_{\mathcal{E}} = \frac{e_{\mathcal{E}}}{\mathcal{E}}, \tag{33}$$

where $e_{\mathcal{E}} = |\tilde{\mathcal{E}} - \mathcal{E}|$ is the absolute error of $\tilde{\mathcal{E}}$ [12].

The results are presented in Figure 3a for Forward Euler with different time steps and similarly for Runge-Kutta 4 in Figure 3b

What is noted from eq. (33) is that the relative errors for Forward Euler decrease with smaller time steps which is expected. For Runge-Kutta 4 the magnitude of error is significantly small, with the highest error at a value of 10^{-12}. This indicates a high level of accuracy and given that minimal error, it is impractical to pursue further comparisons at this scale. Therefore, it is reasonable that comparing errors smaller than this threshold isn't useful for understanding how well the method works or how reliable the results are.

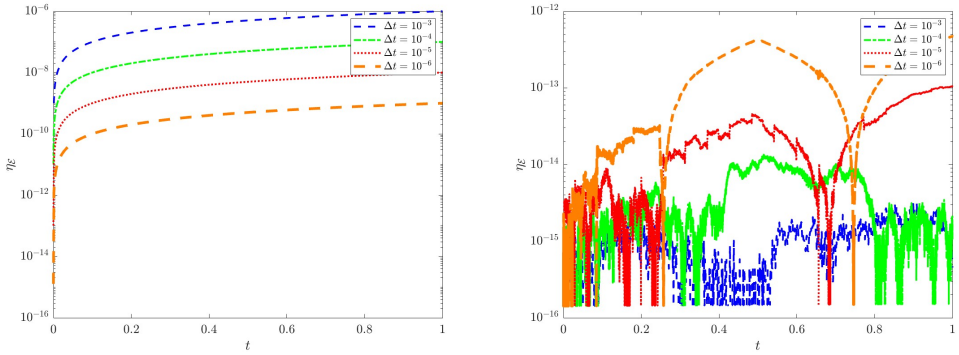

(a) Forward Euler **(b)** Runge-Kutta 4

Figure 3: Relative Error of Numerical results for the linear term with different time steps

Since the relative errors in Figure 3 show very small values, the vorticity field should show a stable behavior. The numerical approximation of the vorticity for both methods is presented in Figure 4. The first plot is the initial vorticity field, the second after a fourth of the simulation time, the third at half of the simulation time, and the fourth at the end of the simulation.

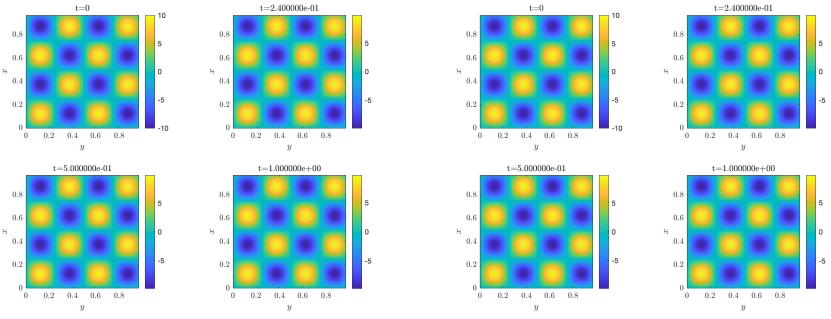

(a) Forward Euler **(b)** Runge-Kutta 4

Figure 4: Numerical result of the vorticity for the linear term with $\Delta t = 10^{-5}, N = 32$ using time-stepping method (a) Forward Euler and (b) Runge-Kutta 4.

Analysis of the change of the field in Figure 4 reveals that it is indeed stable and these methods are considered sufficient for the linear term with the chosen parameters.

5.1.2 Enstrophy for the Non-Linear Term

The non-linear term eq. (15) was analyzed similarly as for the linear term from Section 5.1.1. The constant parameters were set; the kinematic viscosity ($\nu = 0$), the time domain ($T = 1$) and the spatial resolution in each direction ($N = 32$).

When looking at the results for different time steps for Forward Euler and Runge-Kutta 4 in Figure 5 it can be observed that the behavior is not following the manifold. The manifold shows a potential set of solutions that are expected in the tested case and represented by the dashed line in Figure 5.

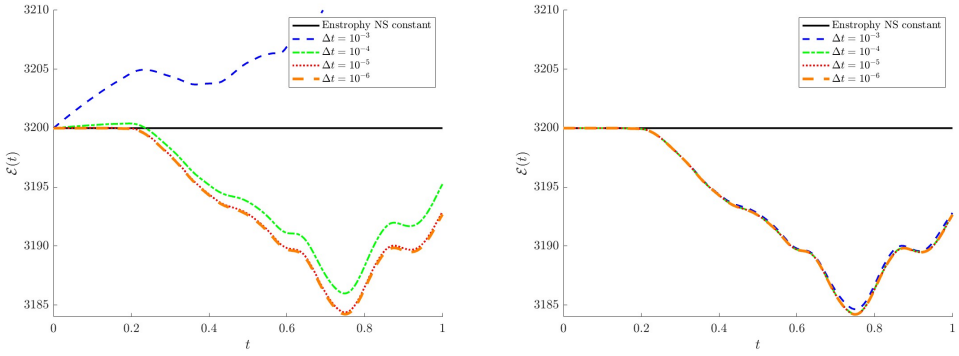

(a) Forward Euler **(b)** Runge-Kutta 4

Figure 5: Numerical result of Enstrophy for the non-linear term with different time steps

The relative errors of both numerical methods are shown in fig. 6 and are larger in comparison to the errors for the linear term.

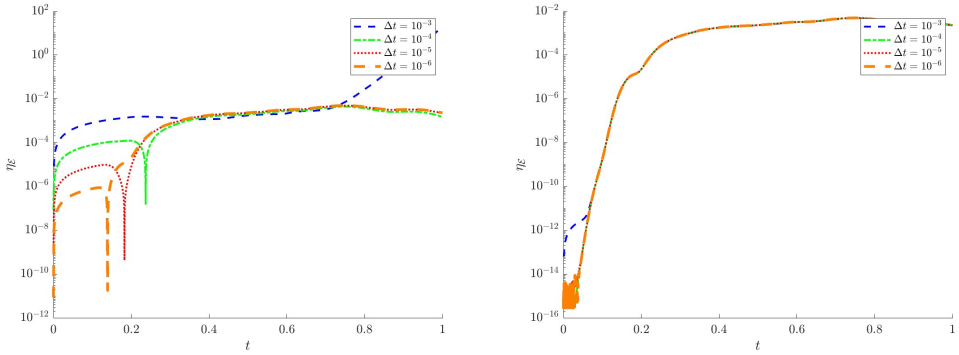

(a) Forward Euler **(b)** Runge-Kutta 4

Figure 6: Relative Error of Numerical results for the non-linear term with different time steps compared to the manifold (constant value of the enstrophy).

It was expected that the relative error compared to the manifold would be greater

than the error for the linear case. What can also be seen in Figure 6 is that smaller time steps do not result in a reduction of errors.

The vorticity field is expected to show different behavior during the running time thus earlier results indicate an unstable behavior. The results are presented in Figure 7.

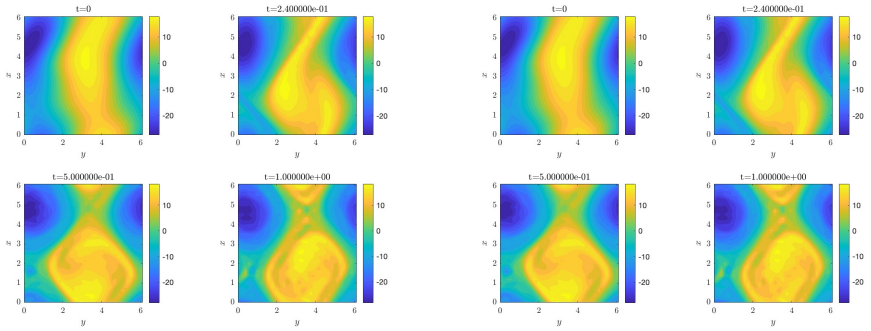

(a) Forward Euler **(b)** Runge-Kutta 4

Figure 7: Numerical result of the vorticity for the non-linear term with $\Delta t = 10^{-5}, N = 32$

As expected, the unstable behavior of the numerical approximation of the vorticity is shown through the vorticities in Figure 7.

5.2 Enstrophy recovering strategy

From Section 5.1.1 and Section 5.1.2 it is clear that only the non-linear term needs a recovery strategy for its enstrophy loss.

The perturbation method from Section 4.1 was implemented here on the non-linear initial condition. What will be presented here is that for some small step h, a new and improved perturbed vorticity could be implemented to achieve improved results due to $|\kappa - 1|$ from eq. (32b) approaching zero. The correlation coefficient was evaluated using various time steps and spatial resolutions to ensure $|\kappa - 1|$ approaches zero with finer increments.

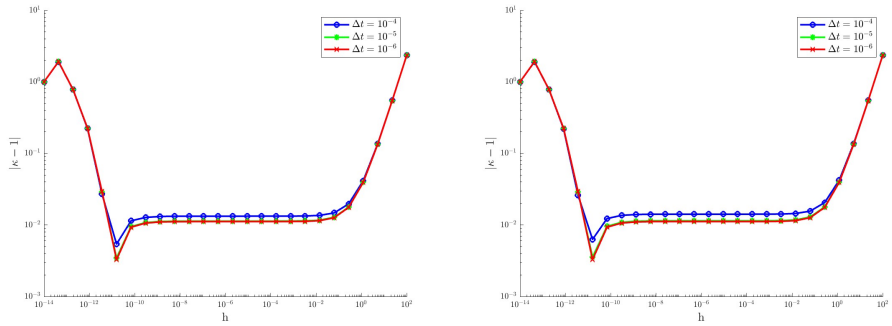

(a) Forward Euler **(b)** Runge-Kutta 4

Figure 8: Results of $|\kappa - 1|$ with $N = 32$, for a range of values h showing refinement of temporal discretization.

Figure 8 shows a similar behavior with the different choice of time steps for both methods. However, what was evident from the plots was that when h were in the order of 10^{-11} the relation coefficient κ was closest to 1.

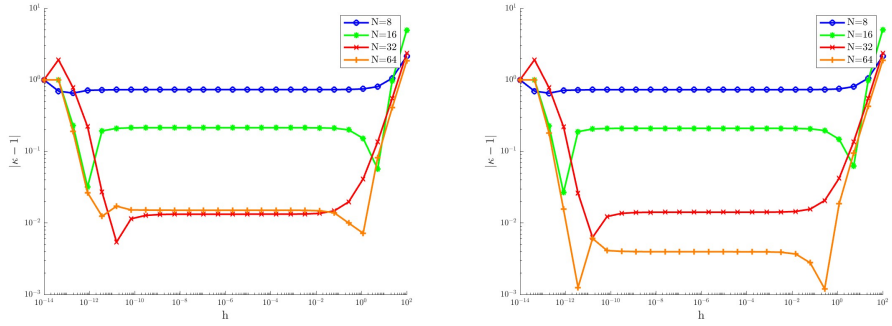

(a) Forward Euler **(b)** Runge-Kutta 4

Figure 9: Results of $|\kappa - 1|$ with $\Delta t = 10^{-4}$

Figure 9 presents the results of κ for the different numerical methods when changing the spatial resolution. As illustrated in the figure, $h = 10^{-11}$ for Forward Euler was the best result, and for Runge-Kutta 4 is either $h = 10^{-11}$ or $h = 10^{-1}$. The best option is to have a spatial resolution as $N = 32$ for Forward Euler and $N = 64$ for Runge-Kutta 4.

6 Discussion & Conclusions

When observing the results from the numerical methods where the kinematic viscosity was greater than zero it was revealed that the enstrophy exhibits exponential decay from Figure 2. This behavior aligns with predictions based on the Taylor-Green vortex solution from eq. (16b). In addition, the measured relative error associated with enstrophy was found to be negligible, indicating that no additional strategies were necessary for conserving the enstrophy. The conclusion for the linear term presented as eq. (14) of the Navier-Stokes was that a simple numerical method such as Forward Euler is sufficient for the conservation of enstrophy with the selected parameters.

Evaluation of the non-linear term presented as eq. (15) was done by setting the kinematic viscosity to zero and using a random vorticity field as an initial condition. The performance of both Forward Euler and Runge-Kutta 4 methods was found insufficient as numerical methods for approximation and conserving enstrophy. To rectify this issue, a perturbation method was implemented as a remedy strategy. Detailed insights into this can be found in Section 4.1. Additionally, the inner product between the perturbation and the random initial condition of vorticity was proven in Section 5.2 very close to zero for both methods. This indicates that a perturbation method is a valid strategy to implement for conserving the enstrophy with a non-conserving numerical method. With this it allows us to characterize the normal component of solutions.

The main objective is to assume that enstrophy conservation is a constraint manifold. By making this assumption, we determine the Gâteaux derivative of the manifold. This allows us to identify the normal component of solutions on the manifold. This enables further studies to construct a retraction operator via adjoint calculus. This study establishes a foundation with perturbations. From that, one can derive the adjoint equations and utilize the Riesz representation theorem to determine an equivalent expression.

The question regarding this recovery strategy is whether obstacles might arise when implemented and if the effort that is required is greater than the reward. That is, would this method be preferred to use over more complex numerical methods that are energy-conserving from the beginning?

7 References

Whole bibliography

[1] A.Palha and M.Gerritsma. *A mass, energy, enstrophy and vorticity conserving (MEEVC) mimetic spectral element discretization for the 2D incompressible Navier–Stokes equations*. Tech. rep. University of Technology Eindhoven, Delft University of Technology, 2016.

[2] G P.Galdi. *An Introduction to the Mathematical Theory of the Navier-Stokes Equations - Volume I: Linearized Steady Problems*. New York: Springer-Verlag, 1994.

[3] A Ramgard. *Vektoranalys*. 2. uppl. Stockholm: Teknisk högskolelitteratur i Stockholm, 1992. ISBN: 9185484350.

[4] *Annual review of fluid mechanics [Elektronisk resurs]*. Palo Alto, Calif., 1969.

[5] *SG1217 Strömningsmekanik Kompendium v.t. 2012 [Elektronisk resurs]*. 2012.

[6] *A BRIEF INTRODUCTION TO VORTEX DYNAMICS AND TURBULENCE [Elektronisk resurs]*. H.K. Moffatt, 2011.

[7] P Matharu. *From Extreme Behaviour to Closures Models — An Assemblage of Optimization Problems in 2D Turbulence*. Tech. rep. McMaster University, 2022.

[8] Z Qu. *Fast Operator Splitting Methods For Nonlinear PDE:s*. Tech. rep. Tulane University, 2016.

[9] TY Hou. *Blow-up or no blow-up? A unified computational and analytic approach to 3D incompressible Euler and Navier–Stokes equations*. Tech. rep. Caltech, Pasadena, 2009.

[10] JB Scarborough. *Numerical mathematical analysis*. 2. ed. Baltimore: Johns Hopkins Press, 1950.

[11] PD Lax. *Functional analysis*. New York: Wiley-Interscience, 2002. ISBN: 0471556041.

[12] L Råde and B Westergren. *Mathematics handbook for science and engineering*. 5., [rev.] ed. Lund: Studentlitteratur, 2004. ISBN: 9144031092.